Journal of Polymer Science and Engineering 2025, 8(1), 4772.
https://doi.org/10.24294/jpse4772

Article

Enhancing non-lethal defense: Advanced high-density polyethylene nanocomposites for projectile holders

Boumdouha Noureddine*, Duchet-Rumeau Jannick, Gerard Jean-François

UMR CNRS 5223 Ingénierie des Matériaux Polymères, Université de Lyon, INSA Lyon, 20, Avenue Albert Einstein, 69621 Villeurbanne, France
*** Corresponding author:** Boumdouha Noureddine, boumdouhanoureddine@gmail.com

CITATION

Noureddine B, Jannick DR, Jean-François G. Enhancing non-lethal defense: Advanced high-density polyethylene nanocomposites for projectile holders. Journal of Polymer Science and Engineering. 2025; 8(1): 4772.
https://doi.org/10.24294/jpse4772

ARTICLE INFO

Received: 21 February 2024
Accepted: 27 May 2025
Available online: 11 June 2025

Abstract: Industrial plastics have seen considerable progress recently, particularly in manufacturing non-lethal projectile holders for shock absorption. In this work, a variety of percentages of alumina (Al_2O_3) and carbon black (CB) were incorporated into high-density polyethylene (HDPE) to investigate the additive material effect on the consistency of HDPE projectile holders. The final product with the desired properties was controlled via physical, thermal, and mechanical analysis. Our research focuses on nanocomposites with a semicrystalline HDPE matrix strengthened among various nanocomposites. In the presence of compatibility, mixtures of variable compositions from 0 to 3% by weight were prepared. The reinforcement used was verified by X-ray diffraction (XRD) characterization, and thermogravimetric analysis (TGA) and differential scanning calorimetry (DSC) were used for thermal property investigation. Alumina particles increased the composites' thermal system and glass transition temperature. Mechanical experiments indicate that incorporating alumina into the matrix diminishes impact resistance while augmenting static rupture stress. Scanning electron microscopy (SEM) revealed a consistent load distribution. Ultimately, we will conduct a statistical analysis to compare the experimental outcomes and translate them into mathematical answers that elucidate the impact of filler materials on the HDPE matrix.

Keywords: non-lethal projectile holders; high-density polyethylene; X-ray diffraction; differential scanning calorimetry; thermogravimetric analysis; scanning electron microscopy; statistical study

1. Introduction

The demand for polyethylene to meet the national market is rising worldwide. Due to its highly crystalline structure, polyethylene is the most rigid and the least versatile of all polyethylene forms. High-density polyethylene (HDPE) has very few branches. The density is, therefore, constantly more significant than 940 kg/m^3. The rigid and somewhat harsh character of a wide range of treatments is proper. Polyethylene materials show viscoelastic behavior, which is approached because their stress response is between the elastic solid and the viscous fluid. The viscoelasticity principle is then implemented as a suitable synthesis of the two ideal behavioral forms.

The polymer of the polyolefin class remains the world's most enormous plastic volume manufactured in various applications [1]. Moreover, the course is among the most versatile thermoplastic polymers, the properties of which can be easily changed or processed [2,3]. Since a 3D structure was developed, in addition to the polymer's dimensional and thermal stability [4,5], this structure offers greater tensile strength, increased stiffness, and chemical resistance [6,7]. It is also affected by temperature and its hydrocarbon solubility [8].

The primary objective of this endeavor is to develop loaded nanocomposites. Natural clay is ideal for reinforcement and is easily removable. They elucidate the fabrication of organic matrix composites to ceramic and metal matrices [9]. In this respect, alumina is an up-and-coming candidate. Its principal particle size is ten nanometers. Alumina agglomerates can be broken during the molten phase in the HDPE case [10,11]. That alumina is scattered in the water, and its subdivisions are distributed separately in the associated watery media. Siengchin et al. [12] used this alumina characteristic and mixed it with polyoxymethylene, polyamide [13], and a PE-based thermoplastic elastomer [14]. Alumina, scattered in the water, was put into the molten polymer and evaporated afterwards. The construction of that extruder screw and the added use of the vacuum pump were facilitated. The alumina level dispersion for the water-based mixture was marginally higher than for the conventional molten mixture for the thermoplastic elastomer [15]. They prove alumina can be incorporated into polyolefins without additional polymer treatment or additives. Polyethylene is the most significant synthetic polymer, which is simple to transform and has an essential shock-absorbing property. It is the best component for making non-lethal projectile holders [16–18].

This research aims to create projectile carriers of high-density polyethylene with the desired properties for a non-lethal application regulated by their physical, mechanical, and morphological characteristics [19]. Also, the thermal properties and effect of the addition of alumina (Al_2O_3) are evaluated, and carbon black (CB) in high-density polyethylene (HDPE) has been integrated to research additive material effect on the consistency of high-density polyethylene projectile holders [19]. We address the development of polyethylene with materials that make it more efficient. Various avenues have been explored to react to this continuous race to increase the properties of materials while maintaining low cost, particularly reinforcing polymer materials using nanometric artefacts [20,21].

Our HDPE mixture blends have been prepared in granules in an extruder. From the multiple tests carried out (fluidity index, density, traction, hardness, impact resistance, and Vicat) on the samples prepared, we could research the impact of the carbon black and alumina rate on the different properties of HDPE mixtures and find the best suitable percentage. Mechanical research seeks to assess the effect of alumina levels on tensile and impact properties. TGA and DSC can be used to determine the effects of various levels of alumina on composite thermal properties. X-ray diffraction (XRD) characterizes alumina used to reinforce composites. SEM microscopy is used to research the influence of alumina on the mixture's morphology. The diagram displays our experimental approach (see **Figure S1** in the support information SM).

2. Experimental methods

2.1. Materials

2.1.1. High-density polyethylene (HDPE)

We chose high-density polyethylene grade PE80 made by CPK2 Skikda, which features colorless and waxed strength. It melts at about 85 °C–140 °C, with a glass transition temperature of −110 °C [22]. The maximum temperature is 120 °C, and the

minimum is 100 °C. The hardness is by SD65, so it becomes crisp at −25 °C. They come from the polymerization of the gaseous ethylene monomer into a homopolymer, developed as a white granule, which was used in this analysis. This grade is appropriate for the manufacture of projectile holders for shock proofing. The main properties of HDPE are shown in **Tables S1–S4** in SM.

2.1.2. Carbon black (CB)

The black carbon used is an ENSACO 250 G type, which the Bental Company provides. It is a powder made of spherical molecules with an average diameter of 45 nm and can cross several hundred nanometers in length and exceed one micrometer. These totals are formed into groups or pools, which is this powder's secondary structure. We used carbon black in this study under Reference (CI 77266, black color) according to CI and CAS No. 1333-86-4 under the Criteria, Equity, Health, and Safety Committee CNSST [23,24]. It is a perfect enhancement. These carbohydrates are used as a pigment/coloring if combined with plastic materials in limited quantities [25]. The characteristics of the carbon black core are seen in **Table S5** in SM.

2.1.3. Alumina (Al_2O_3)

The alumina provided by the rental company, used as reinforcement for high-density polyethylene, has a density of 3.72 g/cm^3, a grain size of 6 μm, white color, a hardness of 45 N at 78 N, and a maximum temperature of 1600/2912 °C/°F. It is a material with a practical, fillable surface, and essential aluminium oxide. By heating it at 150 °C to 350 °C, we can restore the original efficiency of activated alumina. The water in it is removed when the dryer is heated. They mean that activated alumina can be repeatedly regenerated and recycled. The alumina core characteristics are given in **Table S6** in SM.

2.2. Sample preparation

2.2.1. Mixture preparation

We analyzed HDPE/CB and HDPE/alumina mixtures to reach the optimum carbon black and alumina ratio. They were the method of preparing mixtures in a molten state. The proportions of mixtures used are: 100/0%, 99.5/0.5%, 99/1%, 98.5/1.5%, 98/2%, 97.5/2.5%, and 97/3%. Simple HDPE compounds are given in **Table 1**.

Table 1. Essential compounds in the preparation of HDPE.

Mixture	HDPE_1	HDPE_2	HDPE_3	HDPE_4	HDPE_5	HDPE_6
CB % wt	0.5	1	1.5	2	2.5	3
Al_2O_3 % wt						

Note that carbon black and alumina inputs of 0.5% and 3% are in excess. Therefore, mixing well to have a good dispersion of additives in the product HDPE is important. The application of the thermoplastic matrix combined with the carbon black and alumina takes place through two main stages: Extrusion, which allows both components to be blended and extruded in the molded state, and cut into granules, which prepares the plate for various tests by thermal compression. The working

conditions are selected to homogenize the scattering and load distribution in the matrix material without deteriorating the matrix or the load.

It is important to note that our study focuses exclusively on the effect of filler ratios on the characteristics of HDPE composites rather than including an original, unfilled HDPE sample for direct comparison. This approach aims to isolate and analyze the performance changes induced by varying proportions of carbon black and alumina as fillers. Previous studies have established the baseline properties of unfilled HDPE, such as its density, thermal properties, and mechanical behavior, which are used as references in this context [26,27]. The chosen methodology allows for a more precise assessment of the influence of filler content on composite material performance while leveraging existing knowledge about pure HDPE properties [28].

2.2.2. Extrusion

Our HDPE mixture blends have been prepared in granules in an extruder. Products in HDPE granules and (carbon black and alumina) powder are inserted into the extruder in the required proportions for each desired composition according to the following operating conditions in **Table 2**.

Table 2. Extruder lamination chamber operating temperatures.

Screw Rotation Speed (VR) (revolutions/min)			**30**	
The zone	1	2	3	4 (The sector)
Temperature (°C)	150	170	180	180

2.2.3. Compression thermal

This technique was used to process 2 mm, 3 mm, and 6 mm thick plates using a thermo-compression bonding hydraulic press with leaves of the brand IQAP LAP, PLA-30. The material extruded at the extrusion period is placed in the mold over and above two sheets of isolated polystyrene interposed between two sheets of metal and thermally pressed over several phases, as seen in **Table 3**.

Table 3. Working conditions and steps of the hydraulic press.

Initial temperature (°C)			**190**
Cooling rate (°C/min)			**15**
Step	**Time (min)**	**Heat (°C)**	**Pressure (bar)**
1	1	190	10
2	3	190	50
3	7	80	100
4	5	40	50
5	2	30	1

2.2.4. Test specimen's preparation

Standardized test parts that correspond to the acceptable Izod, Vicat, traction, hardness, and density tests are required for HDPE mixtures. The specimens are prepared using notch screw punching and notching machines according to measurements, form specifications, and standards. The ASTM D-256 Izod impact test

uses a pendulum device to measure the impact resistance of materials, commonly applied to plastics and composites.

As per ASTM D256, the samples for measurements are made of a 6 mm thick plate: l = 100 mm and l = 12.7 mm, with a central notch (V) of 2.5 mm wide. Three experiments are performed, and the average value is used in Izod and Charpy's notches unit. The device is CEAST type 6951, its principle is to make a 2.5 mm "V" shaped notch in a test piece of dimension (127 × 12.7 × 3 mm) after preparing them as described in standard ASTM D256 to perform the Izod test. **Table 4** displays the test components prepared from HDPE mixtures in various shapes and sizes depending on their use.

Table 4. Preparation of the various test specimens.

Standards test	**Specimens**	
	HDPE/Alumina	**HDPE/CB**
Vicat/ASTM D1525 standard		
Izod/**ASTM D256 standard**		
Tensile/ASTM D638 standard		

2.3. Characterization of supports HDPE

2.3.1 Physical test

Density at 23 °C

Density of 23 °C is calculated using the CEAST type 6001 ASTM D1505 gradient column technique. The samples to be examined can be washed and weighed. In addition, they are cutting the pieces from the center of gravity of a circle of 2 mm in thickness that has already been molded using a hydraulic press. The samples rinsed with isopropanol are put in the column, and three tests measure their height to assess the average density values [29]. An Excel file is built on the PC for the density calculation formula one, and the apparatus of the two gradient density columns at 23 °C.

$$\text{Density at } 23\ ℃ = \left(\frac{Y}{Z}\right).(B - A) + A \quad (1)$$

With:

Y: The distance between the sample and the low-density float.

Z: The distance between the two floats.

A: Density of the 1st upper float.

B: Density of 2nd lower float.

2.3.2. Thermal characterization

Fluidity index (MFI)

HDPE is extruded onto a 2 mm by 8 mm die at 190 °C, with a 2.16 g load. This test was conducted with a fluid meter, Tinius Olsen model MP600, in compliance with the ASTM 1238 standard. Preheat and clear the plastome cylinder first. Please put in the already cleaned die while testing its diameter. First, preheat to at least 190 ± 2 °C for 15 min before the test. Pour the sample to be analyzed into a cylinder [30], preheat without weight for 3 min and weight for 3 min while releasing air bubbles, and then break this excessive extruder into bits.

Softening temperature (Vicat)

This process was performed according to standard ASTM D1525 to determine the temperature at which a pointed needle carrying 10 N penetrates a standardized sample (10 × 10 × 3 mm) at 1 mm, immersed in a silicone oil bath heated in a CEAST HDT-Vicat unit. The six stations are removed from the tub, the loads are lifted in the bathroom, and the test sample is put beneath the needles of each station. The load is added, the stations are lowered into the bath, the system is turned on, and the sensors are adjusted while they are set to zero. Then, the test is performed. A continuous rise in the temperature is required at a rate of 50 °C/h, and the test is completed. Three trials were conducted for each mixture of compositions. The CEAST HDT-Vicat unit.

2.3.3. Physical-chemical tests

Thermogravimetric analysis (TGA)

ATG Q500 High Resolution works from the ambient temperature until 1000 °C, based on the sample's composition. The analyzer used is of the type TA Q-50 (TA Instruments). The specimens were examined at a temperature increase of 500 °C by a heat threshold of 10 °C/min and then at a flux rate of argon of 40 mL/min. This analysis technique records the variation of a sample's mass as the temperature changes linearly. The pieces to be examined (m_0 = 3 to 5 mg) are put in a precise platinum boat. It's then heated at 1000 °C above room temperature. At the same time, the weight change is calculated as the product degrades. TGA was used in this work to evaluate how alumina content affects HDPE/BC, HDPE/alumina, and thermal stability.

Differential scanning calorimetry (DSC)

DSC differential analyses are a technique that allows observation and measurement of the changes in enthalpy of a substance in a regulated thermal cycle depending on the temperature or time. Relevant heat power with temperature choice modulated DSC Q20 TA instruments has been measured. DSC may be used to assess the thermal transitions of the polymer, i.e., the changes in material properties when the temperature of the material is changed [31]. Two hollows are there. In the first one, "the dug sample," we placed our polymer sample (m_0 = 3 mg). The other one is "the reference," which we leave blank. Each trough has a heater [32]. The summary of the steps is as follows:

- Temperature ramp at 20 °C/min.
- Temperature range: 20 °C to 200 °C.
- Current scanning: Nitrogen (N_2).

The software for the analysis supplied with the device "Universal Analysis" is used to process the data obtained to determine thermodynamic amounts linked to various transitions. Data from the standard graphical analysis software and methods for determining the melting temperature and sample peak areas will be used. By Equation (2), the amount of crystallinity (TC) was defined as follows [33]:

$$TC = \left(\frac{\Delta H_f^{cal}}{\Delta H_f^{\chi}}\right) \times 100 \quad (2)$$

where:

ΔH_f^{cal}: Denotes the measured heat of melting (J/g).

ΔH_f^{χ}: Standard thermal melting points for crystalline HDPE (287 J/g).

X-ray diffraction (XRD)

The system is an X-ray diffractometer, category X'PERT PRO PHILIPS MPD. The X-ray spring is a ceramic tube with an anode made of copper and a 40 KV power supply. The diffractometer equipment consists of a rear sample monochromator with a slit collimator scaling counter. The powder is spread over a flat sample holder using a glass plate to achieve a surface plane and then mounted in the diffractometer [34]. XRD is commonly used to assess their structure and the distance between the sheets in the analysis of clays. However, the XRD analysis was used only to evaluate the existence of the alumina in the composites. This approach involves sending an X-ray beam at wavelength A, directing it at the sample, and analyzing the diffracted signal. For each angle of the beam's incidence, the amplitude of the diffracted signal is the same as the X-ray peak. Suppose a wavelength A x-ray hits at an angle θ to all the reticular planes of the crystalline alumina body, separated by a distance d. In that case, a phenomenon of diffraction occurs from the so-called Bragg law (3):

$$A = 2d \sin\theta \quad (3)$$

With:

A: The beam's wavelength

d: The distance between the levels

θ: The angle of the incident ray

A diagram characteristic is obtained by recording diffraction peaks' proximal upper and intensities [35].

2.3.4. Mechanical tests

Traction uniaxial

Tensile testing is the most frequently used experimental tool in studying mechanical behavior. The test is conducted in compliance with ASTM D638. Tensile testing was performed on a GALDABINI 25 KN style system operated by the software "SUN". The tensile properties of the curves are evaluated. The device is activated, and the software is evaluated for all requisite parameters. The specimen is situated between the two jaws, connected to a force sensor and a movable stretching apparatus, and subjected to tensile forces. From this test, the elasticity of the materials can be obtained, which is seen as the plastic material's potential, without splitting, to deform [36,37]. The larger the *A*%, the more pliable the material is the % extension *A*:

a. If $A\% > 5\%$, the materials are called ductile.

b. If $A\% < 5\%$, the materials are considered fragile or breakable.

Resilience of impact

The impact resistance test following the ASTM D256 standard is performed using a resile impactor-type CEAST system by applying mechanical stress with a high energy impact rate, which leads to a fraction of a second breakdown of a test tube. This test allows the fragility or elasticity of the substance to be deduced under certain experimental conditions. The test part is set with a CEAST notching unit. It is noticed to 2.5 mm in depth and then hammered by 1 joule under the striker's impact, which is attached to the end of a released pendulum and produces a shock. The specimen is destroyed. The characteristic calculated is the resistance to effects (4):

$$a = \mathrm{An}/e(\mathrm{J/m}) \tag{4}$$

where:

a: Resilience to impact (J/m).

An: Average of absorbed energy (J).

e: The thickness of the test piece (m).

The failure form of each sample should be in one of four categories:

C: A break in which the specimen is split into two or more sections (complete break).

H: A break or portion of the sample cannot be assisted over the horizontal when the vertical angle of the other part of the sample is less than 90°, including an incomplete break.

P: An incomplete break is not known as a hinge break, but it breaks at least 90% of the distance from the top to the opposite side (partial break).

K: An incomplete rupture is a fracture where the fracture goes from the top of the notch to the opposite side by less than 90%.

Hardness of Shore D

The Shore D method, developed for rigid polymers, was used for this test, and ASTM D2240 was used for dimensional flats (150 × 150 × 6 mm). The sample was loaded with 4.5 to 5 kg on a CEAST type 6767 durometer needle. Once the hand has been stabilized, the hardness value is read-only. Three sample measurements were made at points around 3 mm apart and about 12 mm from each other at the edge of the sample. The findings are seen in the three experiments on average.

Charpy method

Impact tests are used to characterize the embrittlement of a material. They consist of breaking a notched Charpy test under the impact of a "pendulum." We measure the energy the rupture absorbs, making it possible to return to the material's resilience. Impact resistance characterizes the energy absorbed during the rupture of a smooth or notched bar under the action of a striker endowed with sufficient kinetic energy. A pendulum mass is used. The angle of the rise of the pendulum after the impact makes it possible to calculate the braking energy. Each device generally has several interchangeable pendulums (hammers) corresponding to various energy levels. A range of 0.5 to 50 J applies to all plastics. Shorter length (L = 85 mm). The shock effects of applying mechanical stress at high speed (several meters per second) and

high energy cause a specimen to rupture in a split second. Under given experimental conditions, it allows for judging the fragility of a material-test piece assembly, with the brittleness being synonymous with low elongation rather than low breaking energy. The effect depends on the molecular relaxation process associated with the rupture time, temperature, geometry (notches), and heterogeneity (defects) that generate stress concentrations.

2.3.5. Microstructural characterization

Scanning electron microscopy (SEM)

A JEOL JSM 5800 scanning electron microscope operates at 10 kV. SEM enables the monitoring of the surface morphology of samples with a considerably higher field depth than when exposed to the electron beam in an optical microscope by emissions of secondary electrons, backscattered electrons, Auger electrons, visible photons, ultraviolet UV, infrared IR, X-rays [38]. SEM is a microscopic technique based on interactions between electronics and matter made up of an electron beam scanning the sample's surface and transmitting these particulates. These particles can be examined through various detectors, which allow the reconstruction of a three-dimensional surface picture.

3. Results

3.1. Physical test

3.1.1. The density of HDPE

We obtain the following diagram in **Figure 1** by increasing the density to 23 °C depending on the carbon black and alumina percentages:

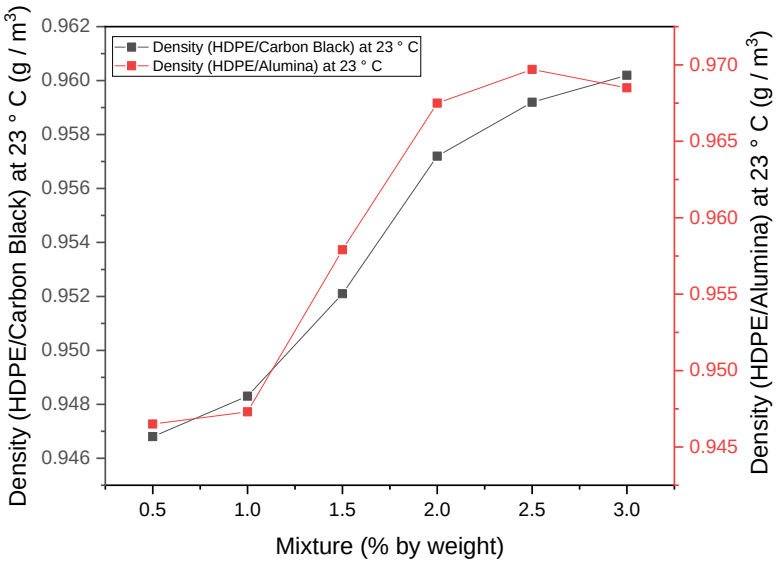

Figure 1. For HDPE mixtures, the density variation at 23 °C is determined by the carbon black and alumina rates.

A variety of findings arise from this analysis. It is worth stressing that the density of HDPE/CB and HDPE/alumina mixtures changes increasingly with increased

carbon black and alumina content, which is clarified by including an extra mass in the neutral polymer.

3.1.2. Resistance to slow cracking in a medium of "stress cracking"

The effects of stress cracking are summarized in **Table 5** below:

Table 5. Stress cracking occurs in HDPE/CB and HDPE/alumina mixtures.

Mixture % wt	0.5	1	1.5	2	2.5	3
Fractional time of the specimens (HDPE/CB) Hour	< 15	< 15	< 15	Test sections crack during the tests.	Test sections break during the tests.	Test sections crack during the tests.
Fractional time of the specimens (HDPE/Alumina) Hour	< 15	< 15	< 15	< 15	Test sections crack during the tests.	Test sections crack during the tests.

According to our stress-cracking findings, these blends have low resistance to slow cracking in a surfactant medium.

The observed density decrease at 3% alumina can be attributed to non-uniform dispersion and agglomeration of alumina particles, which hinder homogeneous matrix formation and increase free volume.

3.2. Thermal characterization

3.2.1. The melt flow index MFI

By taking the MFI as a percentage of the mixture, we get the following graph, **Figure 2**:

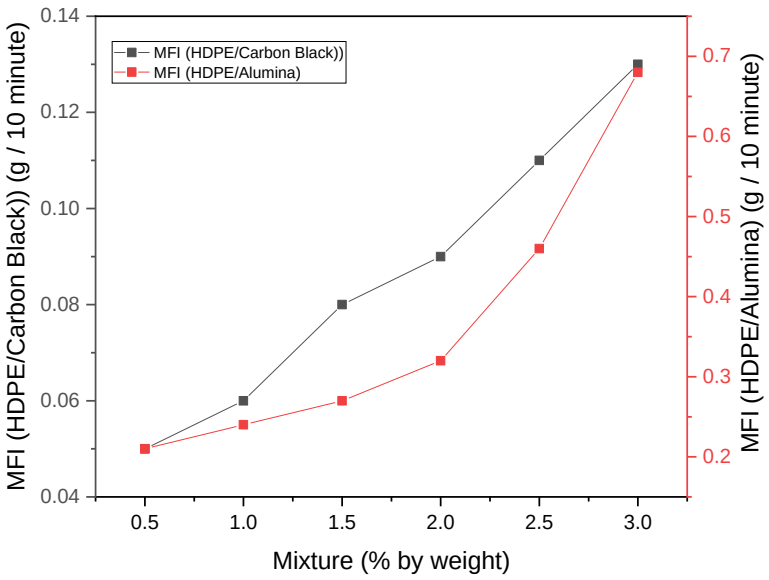

Figure 2. The percentage variance of MFI in the mixture.

Figure 2 indicates a shift in the melt flow index based on the percentage of HDPE/CB and HDPE/alumina mixtures. We observe that at addition rates of 0.5% and 1%, the IF reduced compared to the neutral polymer due to the larger molecular weight of carbon black and alumina in HDPE mixes and their enhanced bonding to long macromolecular chains. For the other percentage, however, the IF is higher than that of neutral HDPE due to grown carbon black and alumina content, resulting in a strong

material flow and, thus, a higher fluidity index, reducing the mixture's viscosity. As the percentage rise in alumina indicates an increase in MFI, we see an increase in processability because MFI indicates polymer viscosity.

3.2.2. Vicat softening point

By increasing the Vicat temperature as a percentage of the mixture, we obtain the following **Figure 3**:

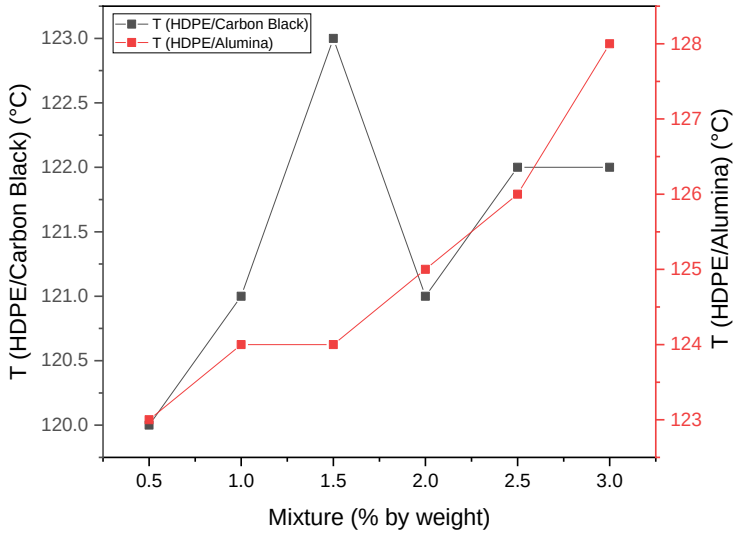

Figure 3. The graph shows the variance of Vicat softening temperature depending on the additive percentage.

Figure 3 demonstrates the temperature fluctuations of the HDPE/CB and HDPE/alumina mixture softening from Vicat. These findings suggest that Vicat's softening temperature is usually due to the chains' flexibility. The percentages rise steadily from 0.5% to 1.5%. The higher value of 1.5% HDPE/CB is explained by the impact strength values of the mixture, but at 2%, we observe a decrease before the temperature adjustment of neutral HDPE. Notice that the temperature for Vicat softening is the same for the neutral resin and the 2% and 2.5%. We conclude that adding carbon black above a 2% point doesn't impact the temperature of Vicat softening. According to these results, the Vicat of HDPE/alumina combination decreases to 0.5% and rises from 1% to 3%.

The increase in Vicat softening temperature at 2.5% carbon black is due to enhanced chain interactions caused by the filler material. However, deviations at higher concentrations indicate non-uniform dispersion effects. Non-uniform dispersion at filler loadings above 3% leads to inconsistencies in the matrix, which are reflected in the anomalies in Vicat temperature measurements.

3.3. Mechanical characterization

3.3.1. Shore D hardness test

The variance in Shore D hardness depends on the mixture percentages, as shown in **Figure 4**.

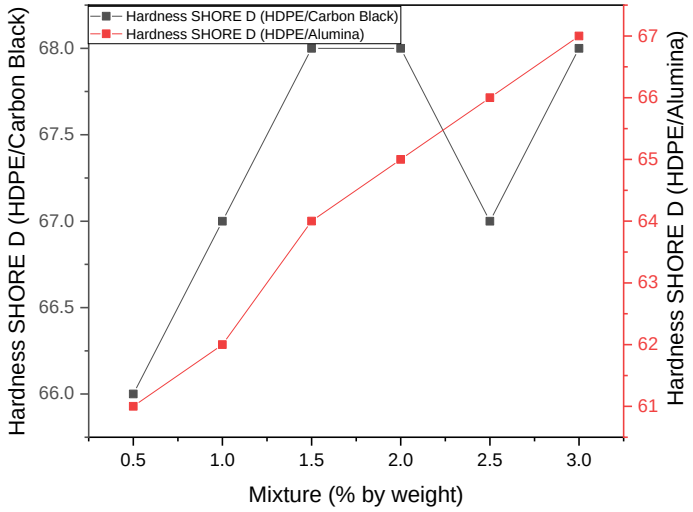

Figure 4. The diagram shows the hardness variance of Shore D as a carbon black and alumina percentage.

Figure 4 shows the hardness difference depending on the black carbon rate for HDPE/CB and HDPE/alumina mixtures. Based on this calculation, it can be noted that the hardness of the neutral HDPE and the HDPE/CB 0.5% mix in carbon black are identical. Carbon black increases hardness by 1%, 1.5%, 2.5%, and 3%, but not 2%. It is concluded that adding carbon black improves the hardness of HDPE. The increase in hardness is slight because of the percentage by weight of alumina, which means that the more the rate of alumina increases, the more deformation resistance increases. The lower impact resistance at 2.5% filler concentration correlates with agglomeration of filler particles, leading to stress concentration points in the composite matrix.

3.3.2. Resistance by Izod impacts

The shift in impact resistance Izod as a feature of the mixture percentage is seen in the following **Figure 5**:

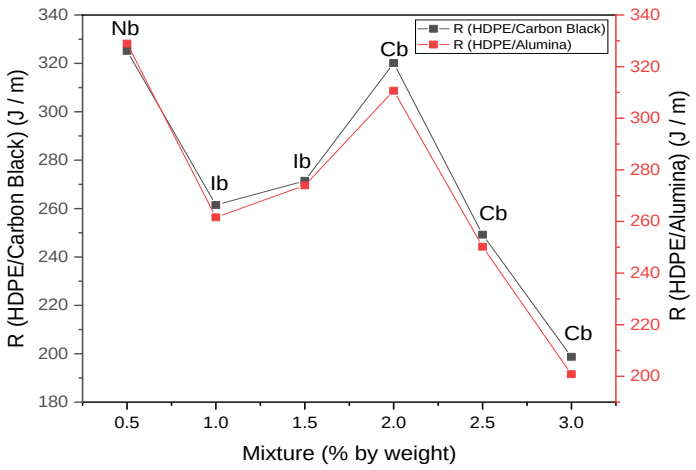

Figure 5. The graph shows the impact resistance Izod resilience difference in carbon black percentage.

Notes: With: **Cb:** Complete breaking; **Ib:** Incomplete breaking; **Nb:** No breaking.

Figure 5 shows the difference in resilience depending on the HDPE/CB and HDPE/alumina levels. It can be understood that the two curves practically overlap, and as the percentage of HDPE/CB and HDPE/alumina mixtures increases, the impact resistance increases. With an incomplete fracture of 50% of the specimen's HDPE. Where a fracture extends less than 90% from the top of the notch to the opposite side of the fracture, at 5% to 1%, the impact resistance of the materials produced decreases compared to virgin HDPE due to the lack of HDPE/CB interaction that favors the interaction of carbon black in particles and leads to increased particle size. In this case, a weaker external force will cause HDPE/CB to break down the material.

However, with carbon black, the impact resistance increases from 1% to 1.5%, which can lighten the interface voltage, better distribute the matrix's phase-part, and augment the material's durability to resist the spread. In carbon black, this increase continues to hit a limit of 2%, which provided better behaviors about impact resistance where there was no breakdown. They are the case with neutral HDPE, representing the dominant HDPE and 2% HDPE/CB in mixture strength characteristics.

Then, the decrease in impact resistance of materials with a high carbon black rate of 2.5% and 3% thus increases the rigidity of the manufactured material considerably, decreasing the impact resistance of carbon black with greater rigidity than HDPE. Writers were caused by the molecular increase in weight and the effect of increasing interfacial tension, resulting in a poor scatter in the matrix of the dispersed phase particles. Moreover, this reduction contributes to the formation of aggregates, which results in low material impact resistance and, therefore, degradation of the strength of the HDPE/CB mixture.

3.3.3. Traction test

Three essential parameters that define the conduct of traction materials can be drawn:

3.3.4. Elastic tensile strength σ

The following diagram displays the results of the ratio of elastic tensile power in carbon black and alumina percentages, as shown in **Figure 6**.

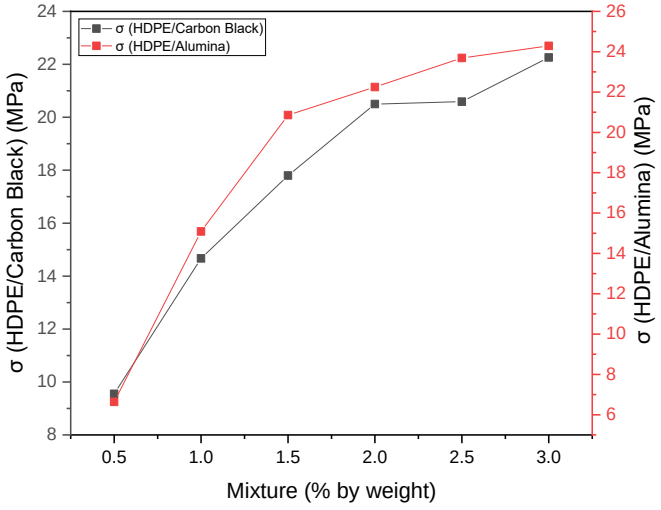

Figure 6. The variation in elastic tensile power in carbon black and alumina percentage.

Figure 6 illustrates the variance of elastic stress to the carbon black feature and alumina concentration. The adjustable tensile strength progressively escalates with carbon black and alumina percentages. The carbon black gradually imparts elasticity to the HDPE, influenced by the characteristics of the chains and the length and entanglement of inter-chain interactions. The yield point of materials produced by the weight of carbon black at 0.5% and 1% is lower than pure HDPE. Writers are consistent with a ductile-break transition in the charged polymer's behavior. The tensile yield usually increases with the carbon black incorporation rate for a 2% to 5% carbon black load. We observe a unity between the two curves, which confirms that polyethylene's behavior is the same with the same proportions of additives due to their participation in mechanical properties.

3.3.5. deformation at the break (ε_r)

The results of the break elongation are shown in **Figure 7**:

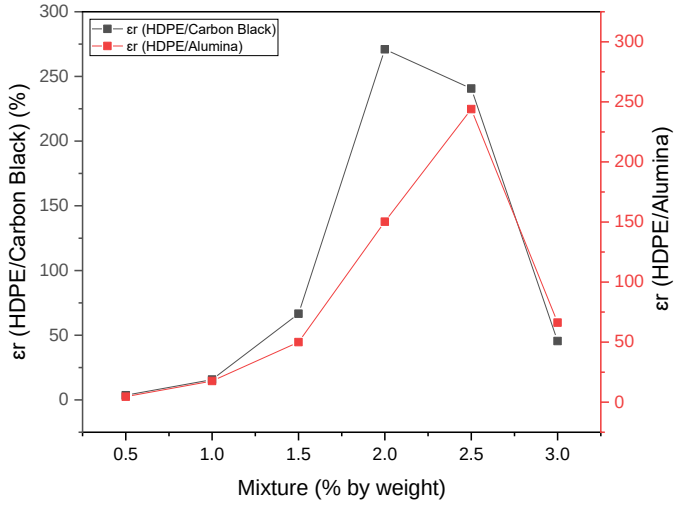

Figure 7. Break elongation (ε_r) differences in carbon black and alumina percentages.

Figure 7 shows the break's elongation difference depending on the carbon black and alumina percentages. HDPE is a highly flexible polymer with more significant deformation than 500% before failure. If carbon black is applied to HDPE, the decrease in the elongation is reduced to $\varepsilon_r < 5\%$ for 0.5% of carbon black, causing the polymer to crack break. Then, we see a difference in the extension of materials formed by the weight of carbon black of 1 to 5% and $\varepsilon_r > 5\%$. They are correlated with the brittle-ductile transformation of colored polymer behavior. The break elongation rises rapidly to 2% of carbon black and has the highest extension of 270.95%. Beyond 2%, deformations decrease, and the matrix and the additive interaction can occur due to strong interactions. Writers lead to a limitation of the movement of interfacial macromolecular chains.

3.3.6. Tensile strength R_r

The Rr tensile strength results are shown in **Figure 8**.

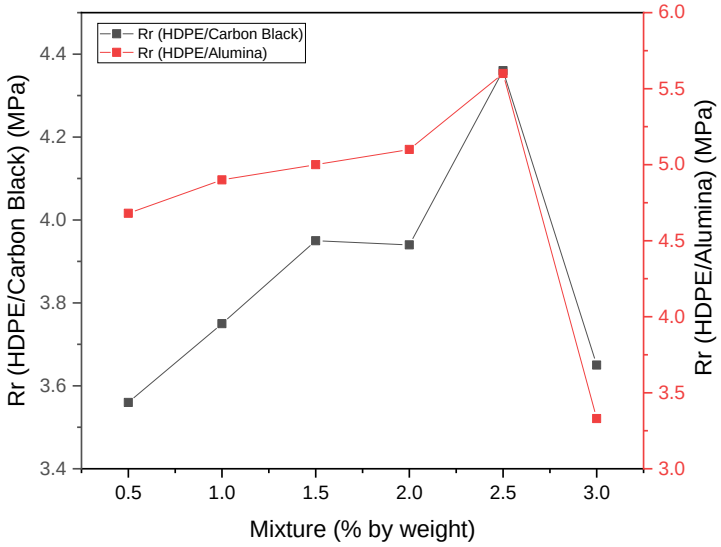

Figure 8. The graph shows the variance of the rupture strength R_r according to carbon black and alumina percentages.

Figure 8 indicates a change in Rr's breaking intensity with the black carbon rate for HDPE/CB and HDPE/alumina mixtures. When the elastic boundary is exceeded, the crystal lattice atoms have switched to the action of an elongation power. In plastic behavior, it is essential to consider crystal defects, particularly dislocations. Adding carbon black and alumina gradually raises its breaking strength to 2.5%, giving us the best breaking strength. Due to increased molecular weight, carbon black gives HDPE the ductility property, leading to new interactive dislocations and interactions. After 2.5%, the tension of the colored material decreases owing to interactions between the matrix and additive. Molecular orientation, weight, crystallinity, and glass transition temperature affect tensile effects [39].

3.4. Physico-chemical characterization

3.4.1. Thermogravimetric analysis (TGA)

Thermogravimetric methods demonstrated a boost in thermal stability. In the presence of alumina, HDPE combinations have a higher degradation temperature. **Figure 9** indicates the mass loss curves of a 2.5% alumina mixture relative to an unfilled HDPE. These findings are consistent with Ling et al. [40]. It can be noted that alumina has become an additional thermo-oxidant stabilizer in nanocomposites. Its influence was quantified by weight loss-based temperature based on traces of TGA. The presence of alumina in polyoxymethylene improves thermal performance [12]. Furthermore, adding alumina has increased polyolefins' stability against photochemical degradation [41,42]. Clarifying the alumina method to boost HDPE and other polymers' thermo-oxidative resilience is complicated and acute.

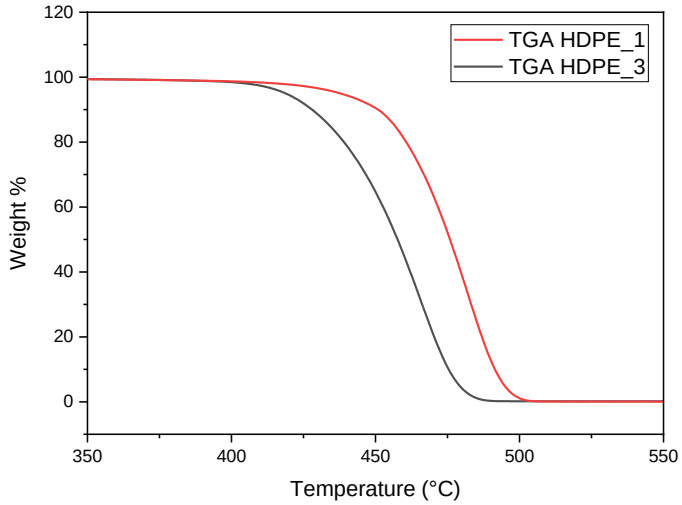

Figure 9. The curve of mass loss without and with load samples.

Both materials undergo deterioration by the identical mechanism of depolymerization, which is a consequence of the breakdown of volatile compounds. The clay-reinforced material exhibits enhanced thermal stability, especially during the initial degradation phase. Certain writers contend that incorporating alumina sheets can improve performance by inhibiting the diffusion of volatile compounds and preventing their leaking into the polymer matrix [43]. They further show that if alumina particles improve a polymer's thermal stability, they act as thermal insulators and, more precisely, as barriers to carrying volatile materials. The degradation temperature increased after adding clay. This thermal stability improvement depends heavily on the polymer blend filler's percentage and dispersion status. The degradation temperature is observed to drop from 421.55 °C to 462.68 °C, a rise of 41.13 °C in the presence of 2.5% clay. This increase is due to a protective surface coating. This result corresponds to Lai et al. [44], whose research on HDPE and alumina nanocomposites demonstrated that the temperature dropped from 330.3 °C for HDPE laden with alumina alone to 412.8 °C for HDPE alone.

Figures 10 and **11** gather composite TGA curves with different filler percentages. The curve form obtained shows similar degradation for all samples: HDPE_2, HDPE_4, HDPE_5, and HDPE_1. The HDPE_3 and HDPE_6 have a slower degradation rate and produce significantly higher residues.

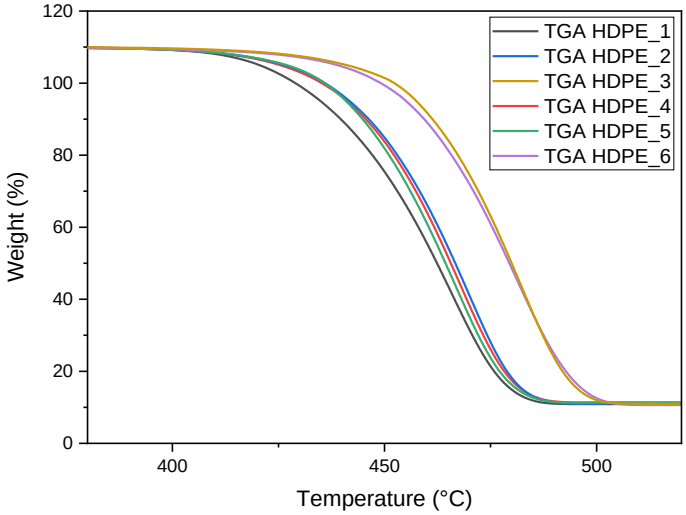

Figure 10. The shift of the % mass loss as a temperature element on TGA curves for different HDPE impact loads.

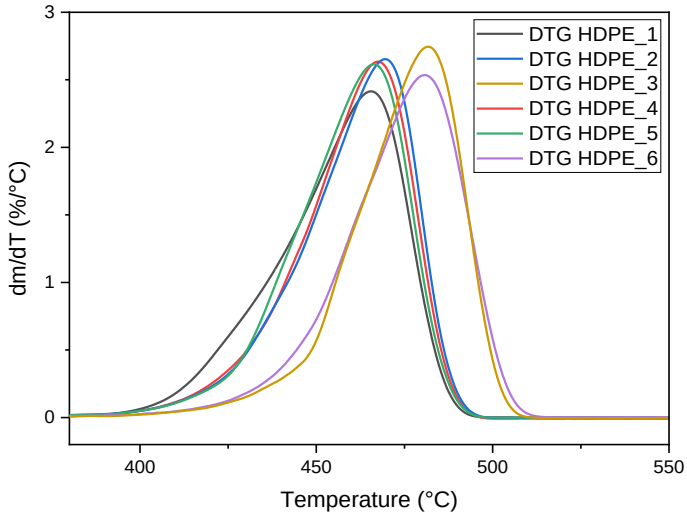

Figure 11. Differential curves, DTG of HDPE.

At a room temperature of about 23 °C, the glass transition temperature of polyethylene is proportional to the filler used [22,45]. With this temperature limit, the weak bonds are beginning to melt, and thermal agitation is necessary to deform the carbon chain [46]. It displays residual masses and degradation temperatures for various HDPE mixtures (**Table 6**).

Table 6. The residual masses and degradation temperatures for different mixtures of HDPE.

Samples	Δm ($m_f - m_0$) (mg)	Loss at the end of the process (%)	Residue at 500 °C (%)	T_{dmax} (°C)
HDPE_1	4.916	100	0.61	465
HDPE_2	4.99	98.79	0.88	467
HDPE_3	5.103	99.33	0.89	468
HDPE_4	4.327	97.14	0.88	466
HDPE_5	4.5479	98.09	0.61	480
HDPE_6	3.432	98.19	0.55	481

3.4.2. Differential scanning calorimetry (DSC)

The DSC thermogram for HDPE in **Figure 12** reveals a melting peak (endothermic reaction). It is observed in the lower section of the thermogram and has been achieved by heating the polymer, directed downward, to illustrate an endothermic melting process. The temperature of melting T_f is determined at the lowest point of the peak, and fusion enthalpy, with the enthalpy for the T_f beginning and T_f, is offset between two temperatures. As these limits are not always easy to find, we used the post-fusion baseline to define the peak of fusion (the peak area). The heating and cooling curves obtained from HDPE, HDPE/CB 2%, HDPE/Alumina 2.5%, and mixtures (1, 2 and 3) are shown in **Figure 12**.

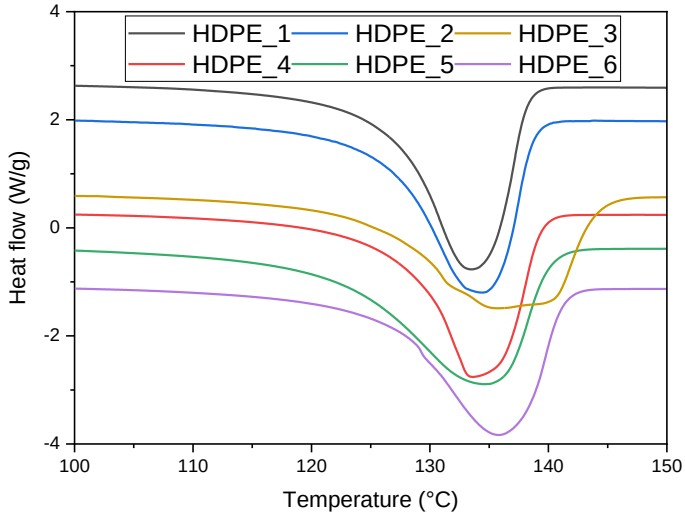

Figure 12. DSC curves for heat indicate the temperature of crystallization melting.

Additives can affect the mixture's glass transition temperature. The effects of alumina on glass transition temperature were observed in thermoplastic polymer matrices due to the influence of alumina pieces on polyethylene chain mobility. These behaviors can contribute to morphology changes depending on the rate of alumina introduction. Leszczyńska et al. made similar observations when studying mechanisms to boost thermal stability with montmorillonite polymer layers [47].

Table 7 presents experimental findings from the DSC thermogram of the six samples, for example, characteristic temperatures T_f and T_c and fusion ΔH_f and ΔH_c enthalpies, along with the degree of crystallinity. Molten endotherms and crystallization exotherms have defined the following parameters:

***T_g*:** Glass transition temperature at which amorphous HDPE changes from hard to soft °C.

***T_m*:** Crystalline fusion space equivalent to heat °C first and second.

***ΔH_f*:** Fusion heat, measured in the region below the endotherm J/g.

***T_c*:** Temperature crystallization is identical to the first and second refrigeration °C.

***ΔH_c*:** Crystallization enthalpy assessed from the exotherm field J/g.

TC: Crystallinity in combinations HDPE % and crystalline HDPE compared to 100% following Equation (2) above.

Table 7. DSC determines the glass transition temperature and melting temperatures of our HDPE.

Samples	T_g °C	T_m °C	TC %	ΔH_f J/g	T_c °C	ΔH_c J/g	Effect
HDPE_1	−107	133	60	125	107	−140	Endothermic
HDPE_2	−106	134	47.6	123	106	−117	Endothermic
HDPE_3	−107	137	63	125	107	−128	Endothermic
HDPE_4	−107	133	52	121	107	−123	Endothermic
HDPE_5	−104	134	44	122	104	−115	Endothermic
HDPE_6	−106	135	45	123	106	−126	Endothermic

The change in glass transition temperature and melting temperature implies a difference in the range of use. The material has the desired temperature in the mechanical component, which shows solid mechanical resistance. The analysis of the DSC allowed an upsurge in the level of crystallinity to be seen, which could be the product of added additives. The melting temperature depends on many factors, including molecular weight, crystallinity, and chemicals [48].

3.4.3. X-ray diffraction

One of our goals is to research composite morphology and properties. Therefore, characterizing alumina is essential. **Figure 13** presents the diffractogram test. The diffractograms obtained for six HDPE samples in this work have nearly similar forms. **Figure 13** shows a standard diffractogram obtained for HDPE in this work. The general format is consistent with the literature for polyethylene diffractograms. Characteristic peaks are well-defined for polyethylene at diffraction angles of 21.4°, 23.8°, and 36.5°. The intensities of such additional peaks, present in some and not others, can be due to the samples of fillers, additives, and antioxidants. The x-ray diffractograms of these analyzed samples were identical in form. They show that the basic crystalline structure is the same for all these samples. Variations in the method of manufacture subject to these samples can, therefore, not influence the crystalline structure. However, many physical processes can modify a polymer sample's crystallinity. Any combination of these may change the finished product's crystallinity.

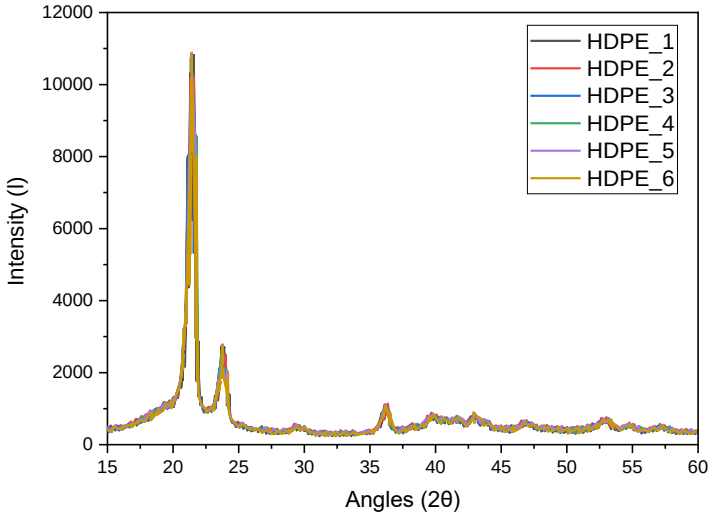

Figure 13. Diffraction of X-ray curves of HDPE.

In the six samples of the HDPE mixture, a weak diffraction peak at 26° was present only in sample HDPE_3. The '*d*' value calculated for this diffraction angle is 3.396 A. For this diffraction angle, no diffraction peak would be detected in specimens HDPE_1, HDPE_2, HDPE_4, HDPE_5, and HDPE_6. The diffraction peaks at 21.4°, 23.8°, 29.5°, 30.5°, and 36.5 ° were detected in all the HDPE samples manufactured in **Table 8**.

Table 8. The distance interplanar D is the relative intensity I for 06-angle samples of HDPE.

Sample	21.4		23.8		26		29.5		30.5		36.5	
	D A	I %	D A	I %	D A	I %	D A	I %	D A	I %	D A	I %
HDPE_1	4.121	100	3.725	22.26	*	*	3.042	1.94	2.958	0.89	2.472	7.44
HDPE_2	3.931	100	3.569	16.6	*	*	2.994	14.71	2.845	0.74	2.405	7.66
HDPE_3	3.935	100	3.555	20.73	3.396	0.57	3.014	3.85	2.93	3.92	2.407	6.73
HDPE_4	4.041	100	3.639	20.42	*	*	2.979	2.25	2.934	1.16	2.447	6.67
HDPE_5	4.306	100	3.887	21.25	*	*	3.05	1.35	2.969	2.82	2.538	7.22
HDPE_6	4.021	100	3.634	17.41	*	*	3.065	0.67	2.937	1.36	2.438	6.17

The XRD results show that each sample's "*d*" values are not unique. They indicate that each piece was made using a different manufacturing process. Also, comparing XRD data from the output of the six HDPE samples is instructive for the extra peaks in the XRD spectrum. The findings of this study show that the presence of additional peaks at various diffraction angles in the XRD spectrum of HDPE is due to the change in the manufacturing method and the various additives and proportions in the samples. Thus, it is possible to infer that the accepted XRD HDPE studies show HDPE sample characterization using the data obtained for six identical HDPE samples. HDPE and alumina 2.5% weight show that the polyolefin matrices have proper clay exfoliation. The findings are consistent with previous results [49–51]. The XRD analysis revealed changes in crystallinity due to filler addition, particularly a shift in the diffraction peaks corresponding to increased interlayer spacing. This effect is indicative of partial alignment and interaction between the filler and the HDPE matrix.

3.5. Microstructural characterization

3.5.1. Scanning electron microscopy (SEM)

Scanning electron microscopy allows the compatibility effect to be obtained, on the one hand, and direct observation of the diffusion of polymer matrix charges. This study helps identify and partly understand the phenomenon causing poor quality of mechanical properties. These depend on the mixture's composition, processing methods, and thermomechanical background. To observe the microstructure and compare the distribution of alumina fillers in the HDPE matrix, we choose HDPE_1, HDPE_3, and HDPE_5, which contain 0.5, 1.5, and 2.5 weight alumina fillers, respectively, as seen in **Figure 14**.

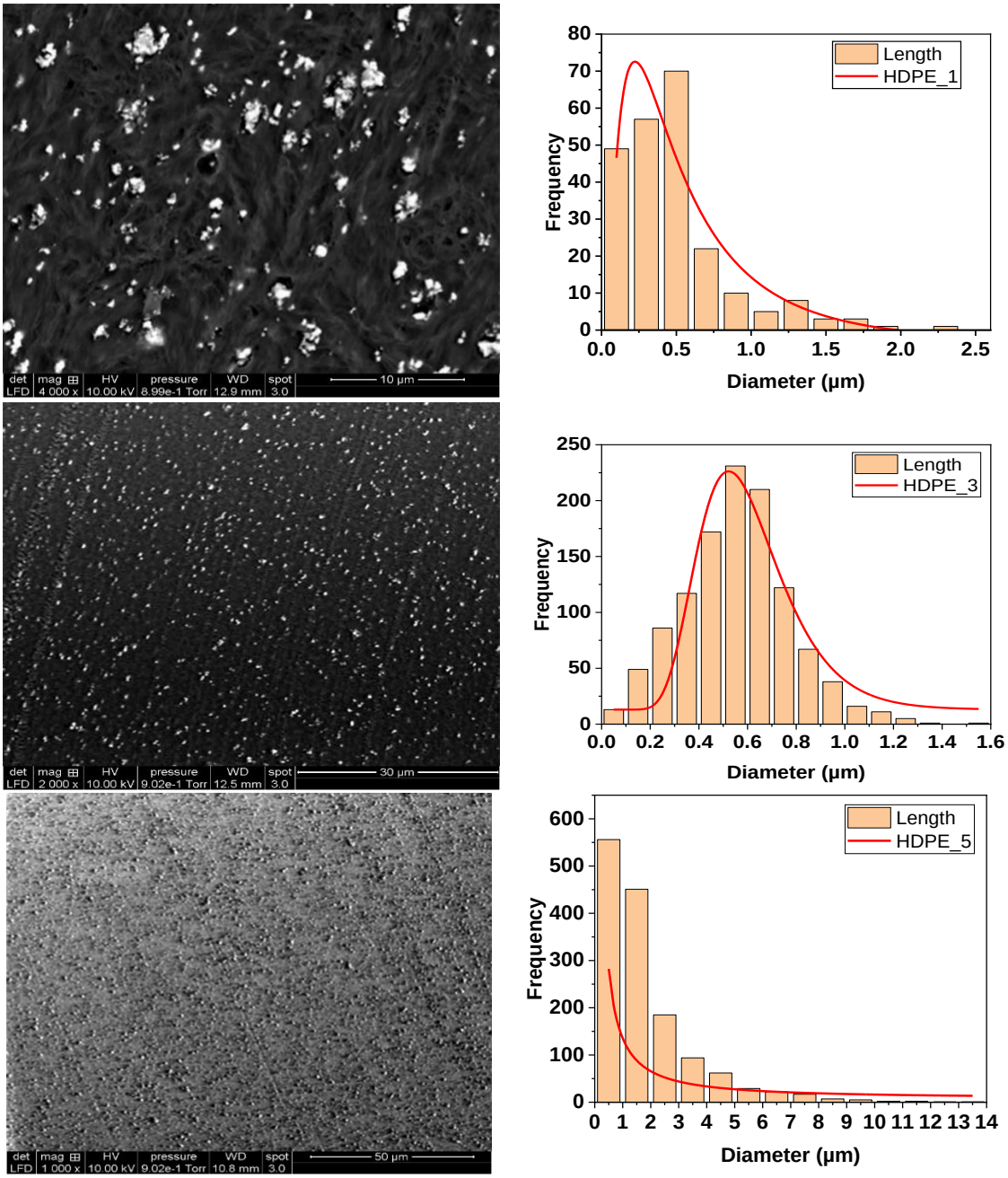

Figure 14. SEM micrographs were taken from a mixture of HDPE_1, HDPE_3, and HDPE_5 alumina weighing 0.5%, 1.5%, and 2.5% by weight, and a histogram of the distribution of the mean filler alumina diameter in various produced HDPE.

Figure 14 depicts SEM images of a mixture of HDPE_1, HDPE_3, and HDPE_5 alumina weighing 0.5, 1.5, and 2.5% by weight. Alumina can be shown to be refined and evenly distributed in the matrices. Alumina remains in fine dispersion when added in more significant quantities, as shown in HDPE_3. HDPE demonstrates the high magnification SEM image where the alumina particles are already agglomerated. Their average size is submicrometric; hence, their compounds are nanocomposites.

3.5.2. Descriptive statistics microstructural

We summarize the distribution of the HDPE, and the filler is given in **Table 9**.

Table 9. Calculation of radii values of filler alumina materials in matrices nanocomposites HDPE.

Mixture	Alumina (% wt)	Dimensions	Minimum	Maximum	Mean
HDPE_1	**0.5**	**Diameter (μm)**	0.03	2.38	0.487
		Area (μm^2)	0.001	0.29	4.292
HDPE_3	**1.5**	**Diameter (μm)**	0.08	1.56	0.557
		Area (μm^2)	0.005	1.93	0.282
HDPE_5	**2.5**	**Diameter (μm)**	0.16	13.14	1.829
		Area (μm^2)	0.02	135.67	5.008

4. Statistical study

4.1. Estimating linear regression for study tests

Linear regression was conducted for each study test utilizing carbon black and alumina within the HDPE matrix to identify the optimal alternative for maximizing performance in this process. This is accomplished by estimating the linear regression for each test individually. Utilizing the Linear Programming matrix enables the attainment of the largest feasible quantity to optimize performance across all tests conducted in this study.

4.1.1. Estimating the linear regression for all tests that rely on carbon black in the filler

Table 10 summarizes the results of linear regression estimation for all tests that were layered using carbon black, and the results were as follows:

Table 10. Estimation of linear regression for tests based on filling with carbon black *R*-sq.

	Coef	*P* value	*R*-sq
Density/CB			
Intercept	0.946	0.000	0.7714
Mixture (M)	0.0051	0.021	
MFI/CB			
Intercept	0.0306	0.001	0.9882
Mixture (M)	0.032	0.000	
T/CB			
Intercept	120.4	0.000	0.3143
Mixture (M)	0.6285	0.247	
D/CB			
Intercept	66.3333	0.000	0.4286
Mixture (M)	0.5714	0.158	
R/CB			
Intercept	332.8667	0.001	0.4922
Mixture (M)	−35.5428	0.120	

Table 10. (Continued).

	Coef	*P* value	*R*-sq
O/CB			
Intercept	9.1606	0.004	0.8963
Mixture (M)	4.8005	0.004	
e/CB			
Intercept	−2.4	0.983	0.2453
Mixture (M)	62.2285	0.318	
Rr/CB			
Intercept	3.6413	0.000	0.1794
Mixture (M)	0.1297	0.403	

Note: Output by Stata 15.1.

We note from the results of the linear regression estimation for the test that applied carbon black that the estimates of the independent variable Mixture (M) were significant for the Denstiy/CB, MFI/CB, and O/CB tests, and this indicates that the estimates are close to being correct with reality. However, for the T/CB, D/CB, R/CB, e/CB, and Rr/CB tests, the independent variable Mixture (M) was not significant. This is due to the instability of the values of the results of these tests. This means that the results are estimates of these tests. It does not accurately approximate reality. Looking at the value of the coefficient of determination (*R*-sq), we note that most of the tests that can be said to be estimated well by linear regression are Denstiy/CB, MFI/CB, and O/CB, as the coefficient of determination exceeded the values of 70%.

4.1.2. Estimating the linear regression for all tests in which alumina was applied in the filler

The linear regression estimation results for each test, depending on the amount of alumina in the filler, are compiled in **Table 11**. The following were the outcomes:

Table 11. Summarizes the results of linear regression estimation for all tests in which the filler was applied using alumina, and the results were as follows.

	Coef.	*P*-value	*R*-sq
Density/Alumina			
Intercept	0.9453	0.000	0.6312
Mixture (M)	0.0102	0.059	
MFI/Alumina			
Intercept	0.0573	0.481	0.8416
Mixture (M)	0.1748	0.010	
T/Alumina			
Intercept	121.8	0.000	0.9143
Mixture (M)	1.8285	0.003	
D/Alumina			
Intercept	59.8666	0.000	0.9844
Mixture (M)	2.4571	0.000	

Table 11. (*Continued*).

	Coef.	*P*-value	*R*-sq
R/Alumina			
Intercept	333.9333	0.000	0.5581
Mixture (M)	−36.3428	0.088	
O/CB			
Intercept	7.2593	0.073	0.4029
Mixture (M)	6.5965	0.013	
e/alumina			
Intercept	−20.6	0.794	0.8212
Mixture (M)	62.3428	0.176	
Rr/Alumina			
Intercept	5.2233	0.002	0.1003
Mixture (M)	-0.26	0.541	

Note: Output by Stata 15.1.

The results of the linear regression estimation for the tests utilizing alumina indicate that all estimations of the independent variable Mixture (M) were significant across all tests. This indicates that the estimates are close to being true to reality, except for the two tests e/alumina and Rr/alumina. This is done by reading the significance value (*P*-value), which was more significant than 0.10, and this indicates a weak linear regression estimate of the reality of the values of these two tests. Looking at the value of the coefficient of determination (*R*-sq), we note that most of the tests that can be said to be estimated well by linear regression are MFI/alumina, T/alumina, D/alumina, and e/alumina. The coefficient of determination exceeded the value of 80%.

4.1.3. Estimate the linear regression for all tests containing pure HDPE

The table below summarizes the results of linear regression estimation for all tests applied to pure HDPE. The results of the tests were as follows:

Table 12. Estimating the linear regression for all tests applied to pure HDPE.

	Coef.	*P*-value	*R*-sq
mg			
Intercept	5.5048	0.000	0.6701
HDPE	−0.2720	0.046	
loss			
Intercept	99.924	0.000	0.4996
HDPE	−0.3811	0.116	
Residue			
Intercept	0.8486	0.006	0.1362
HDPE	−0.032	0.471	
T			
Intercept	459.4667	0.000	0.7329
HDPE	3.3428	0.030	

Table 12. (*Continued*).

	Coef.	*P*-value	*R*-sq
T_g			
Intercept	−170.2667	0.000	0.2530
HDPE	0.3142	0.309	
T_m			
Intercept	133.7333	0.000	0.0454
HDPE	0.1714	0.685	
T_c			
Intercept	61.6133	0.001	0.4218
HDPE	−2.7657	0.163	
H_f			
Intercept	124.8667	0.000	0.3217
HDPE	−0.4857	0.240	
T_e			
Intercept	107.2667	0.000	0.2530
HDPE	−0.3142	0.309	
H_c			
Intercept	−132.9333	0.000	0.2327
HDP	2.3142	0.333	

Note: Output by Stata 15.1.

We note from the results of linear regression estimation for the tests applied to pure HDPE material that all estimates of the independent variable Mixture (M) were not significant for all tests, and this indicates that the estimates are not close to validity in all cases except for the mg test. This is done by reading the significance value (*P*-value), which was less than 0.10. This indicates the approach to estimating linear regression to the reality of the values of these two tests in a significant way. By looking at the coefficient of determination (*R*-sq) value, we notice that most of the tests that can be said to be regression Linearity estimated it well for both mg and T, as the coefficient of determination exceeded 67%. This indicates the importance of fillers in HDPE.

4.2. Results of the Linear Programming matrix

To choose the best mixture that achieves the best results for the experiments applied based on carbon black and alumina, and also to determine the best result for HDPE. The Linear Programming matrix was relied upon to achieve the maximum possible amount. The restrictions of the matrix extracted from the linear regression estimates for the best experiments that we obtained are presented in the following table:

Table 13. Matrix linear programming constraints results obtained.

Matrix constraints		
HDPE	**Alumina**	**HDPE**
		$0.2720\ HDPE_n \leq 0.4018$
$0.0102\ M_{wt} \leq 0.0247$	$0.0051\ M_{wt} \leq 0.014$	$-0.3811\ HDPE_n \leq 0.076$
$0.1748\ M_{wt} \leq 0.6227$	$0.32\ M_{wt} \leq 0.994$	$-0.032\ HDPE_n \leq 0.0414$
$1.8258\ M_{wt} \leq 6.2$	$0.6285\ M_{wt} \leq 2.6$	$3.3428\ HDPE_n \leq 21.5333$
$2.4571\ M_{wt} \leq 7.1334$	$0.5714\ M_{wt} \leq 1.67$	$-0.3142\ HDPE_n \leq 0.2667$
$-36.3428\ M_{wt} \leq -5.9333$	$-35.5428\ M_{wt} \leq -7.8667$	$0.1714\ HDPE_n \leq 3.2667$
$6.5965\ M_{wt} \leq 17.0307$	$4.8005\ M_{wt} \leq 13.0994$	$-2.7657\ HDPE_n \leq 1.3867$
$62.3428\ M_{wt} \leq 269.6$	$62.2285\ M_{wt} \leq 272.4$	$-0.4857\ HDPE_n \leq 0.1333$
$-0.26\ M_{wt} \leq 0.3677$	$0.1297\ M_{wt} \leq 0.7187$	$0.3142\ HDPE_n \leq 0.2667$
$M_{wt} \leq 3$	$M_{wt} \leq 3$	$2.3142\ HDPE_n \leq 7.0667$
$M_{wt} \geq 0$	$M_{wt} \geq 0$	$HDPE_n \leq 6$
		$HDPE_n \geq 0$
Solution of Matrix Maximization		
2.73	2.42	0.85
Decision on the optimal solution		
Mixture % wt = 2.5	Mixture % wt = 2.5	HDPE 1

Note: 1. Outputs via QM software; 2. The constraint indicated in red has been deleted because it restricts the results of the Linear Programming matrix.

The findings of the Linear Programming matrix indicate that maximization was attained from the experimental values applied to the mixture of carbon black and alumina and pure HDPE. The result was that the best mixture was when we relied on carbon black as a filler, according to the result of the Linear Programming matrix, which was estimated at 2.73, which is approximately the mixture at Mixture = 2.5. As for alumina, the Linear Programming matrix estimated the best mixture to be 2.42, approximately mixture = 2.5. Here, a convergence between carbon black and alumina can be observed in the results as the best choice for the mixture that achieves the best results for the applied experiments. Therefore, it is necessary to compare them to determine which material is better between them as the best filler. Pure HDPE was the best result, as the Linear Programming matrix estimated it to have a value of 0.85, approximately HDPE 1.

4.3. Comparison between filling with carbon black and alumina

After determining the best alumina and carbon black mixture, the Linear Programming matrix estimated the best mixture ratio as Mixture = 2.5. We compare the tests and their results at Mixture = 2.5 to determine which is better. The results are shown in the following **Table 14**:

Table 14. Comparison between filling with carbon black and alumina at Mixture = 2.5.

Mixture = 2.5		
Experiments	**CB**	**Alumina**
Density	0.96	0.97
MFI	0.11	0.46
T	122	126
D	67	66
R	249	250
o	20.59	23.69
e	240	244
Rr	4.36	5.6

We can summarize the results considered in **Figure 15**, based on EViews 12 software:

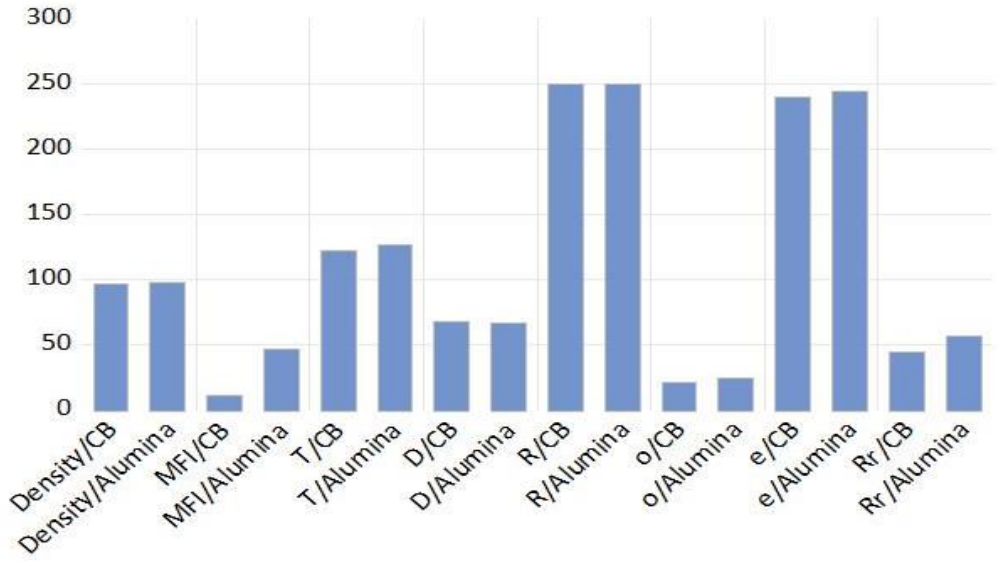

Figure 15. Comparison between filling with carbon black and alumina at Mixture = 2.5.

The results of the experiments applied to both carbon black and alumina materials at a mixture ratio (Mixture = 2.5) are shown in the figure above and in my table. We notice that alumina is superior to carbon black in all experiments except experiment D, which is superior to carbon black but by a negligible difference. Hence, it can be said that alumina is the most stable material compared to carbon black for all experiments. Details of the statistical study and the start of the software work on the main properties of HDPE, alumina fillers, and carbon black are shown in the supplementary materials in **Tables S7–S22** in the SM. These experiments offer additional information regarding the statistical analysis performed on HDPE, alumina, and carbon black mixtures. The linear regression equations confirm that alumina's inclusion in the HDPE matrix leads to a stronger and more stable composite material. On the other hand, when carbon black is used as a filler in HDPE, the results are mixed;

some properties, such as the melt flow index (MFI), get better, but others, like impact resistance, do not improve much when more carbon black is added.

Table S23 in SM shows the linear regression equations used to study the leftover masses and breakdown temperatures of various HDPE mixtures. The data suggests that alumina enhances the thermal stability of HDPE, with higher filler concentrations improving degradation temperatures. However, concentrations above certain thresholds (e.g., 3%) lead to a decline in mechanical properties, such as impact resistance and elongation, likely due to agglomeration effects. On the other hand, black carbon incorporation also improves hardness and impact resistance up to certain percentages. However, excessive amounts may lead to negative interactions between the filler particles and the polymer matrix, reducing overall material performance. The regression analysis confirmed that both alumina and carbon black contributed positively to the mechanical strength of the composites, although the optimal concentration varied for each filler type.

Figures S2–S10 in SM show the results of the linear programming analysis for carbon black and the matrix for alumina. The linear programming matrix reveals that the optimal mixture ratio for carbon black (CB) and alumina is approximately 2.5% by weight, both yielding strong results. Specifically, the matrix value maximizes at 2.73 for carbon black and 2.42 for alumina. Alumina's addition enhances the thermal stability of HDPE, improving its resistance to oxidative degradation and elevating its glass transition temperature. However, excessive alumina (>3%) tends to negatively impact mechanical properties such as impact resistance. In comparison, carbon black improves hardness and impact resistance, with an optimal concentration of around 2%, yielding the best performance.

5. Production of non-lethal projectile holders

After defining the final product composition of the non-lethal projectile holders, we designed and manufactured these holders based on nanocomposites and high-density reinforced polyethylene. In addition to installing the non-lethal projectile heads consisting of polyurethane foams [52–54] in the HDPE holders, the corresponding image shows the expected shape of the non-lethal projectile [55]. Design non-lethal projectile mounts with optimum physical and chemical properties. We have carefully created non-lethal projectile holders by combining high-density polyethylene (HDPE) with nanocomposites to improve their physical and chemical qualities. By carefully adding materials like alumina (Al_2O_3) and carbon black (CB) in different amounts, we have greatly improved how well the HDPE works. Alumina helps the material withstand higher temperatures and resist damage from heat and oxygen, which is crucial for non-lethal uses. It also facilitates the creation of a more robust polymer structure by improving crystallinity and adjusting the glass transition temperature of HDPE. In contrast, the addition of carbon black improves mechanical properties such as hardness and impact resistance, making the material more resilient under stress. However, the addition of excess carbon black can negatively impact some properties, such as elongation and fluidity index, which must be carefully controlled for optimal material performance.

6. Conclusions

The study aimed to develop relations among the composite chemical and microstructural properties based on the thermoplastic matrix and a load of HDPE/CB and HDPE/alumina mixtures. The research focused on polyethylene carbon black and alumina-based composites. Adding carbon black and alumina to the resin remarkably impacts composite material characteristics. They help to increase yields and the young module. An interface region can reduce composite deformation due to the coupling between the filler and the polymer. The hardness research has shown that the filler's surface treatment plays a significant role, affecting the mixture dispersion of particles and adhesion between them. When the physical properties calculated by density are used, the changes achieved reflect relatively good interface efficiency.

The optimal distribution of carbon black and HDPE mixture homogenization varies based on the concentration of carbon black and the conditions of mixing and extraction. During the second stage, molten thermo-compression molding produces the specimens for each test. Various experimental procedures are employed to prepare standard samples for characterization testing. The final stage pertains to the practical techniques for defining materials through physical, thermal, and mechanical testing of HDPE mixes.

Alumina was introduced into HDPE by mixture in the molten state, up to 3% by weight. Alumina is fine and evenly distributed in the corresponding HDPE, though agglomerated. The alumina was well dispersed because the gap between HDPE's melting and crystallinity temperature was significantly reduced. Filling with alumina greatly enhanced the resulting HDPE matrix's thermo-oxidative degradation intensity. The stabilizing effect of alumina on HDPE was more significant. This result is possibly linked to the uptake of the HDPE chain on the alumina surface instead of to the synergistic effect of alumina in the HDPE corresponding thermal stabilizer.

The density of the HDPE mixtures at 23 °C was discovered to be 2%–2.5% carbon black (0.951–0.955 g/cm^3), which is a perfect ratio. Then, it was found that thermal properties such as the HDPE/CB fluidity index remained normal (0.09–0.013) for 2% to 3% black carbon percentages. However, the Vicat temperature of the neutral resin softening and HDPE/CB mixtures are average (122–127 °C), except for 0.5% and 1% of the black carbon percentages. The mechanical characteristics of HDPE/CB mixtures have shown that adding black carbon increases our materials' hardness, which often meets the standards (61–67 Shore D). For the 2% carbon black, the Izod impact resistance results gave a more durable material than other percentages. For the traction, changes in elastic tensile strength depending on the HDPE/CB mixture's carbon black rate gradually give HDPE elasticity properties. HDPE is a flexible polymer whose deformation exceeds 500% before breakage but changes its behavior using carbon black. The 2.5% mixture of carbon black has the best elongation, which explains the material's rigidity.

Different HDPE compound nanocomposites have been studied in dispersion and morphology. SEM better observes the bulk dispersion quality. Surface morphological imaging of nanocomposites by the uniform, non-contact distribution of alumina aggregates on the polymer surface. Also, some variations were observed in surface lamellas' orientation and surface ruggedness between nanocomposites and HDPE

reference films. According to SEM, dispersion efficiency ranged from the dispersal of alumina nanopowder at a mainly nanoscale to the very uneven dispersion of alumina particles at the nano-to-micron scale. Alumina nanocomposites lower HDPE matrix crystallinity and raise peak melting temperatures. An extended DSC melting rise and a substantially increased HDPE/alumina glass transition temperature, respectively.

Supplementary materials (SM): Work methodology flowchart; The image represents a representative granule of HDPE; Automatic hydraulic press representative photograph; Representative photo of a single-screw extruder; ASTM-256 Izod Charpy resilience pendulum-type shock device; Device for making Izod and Charpy notches; Cutting machine tools; Specimens according to ASTM D256 for the Izod impact test; The two gradient density column apparatus at 23 °C; Melt flow index apparatus; The Vicat temperature measurement device is softening. TGA Schematic TA Q500; Measurement of specific heat DSC equipment (a) DSC Qu20, (b) Schematic; a) X-ray diffraction machine b) X Pert PRO MPD diffractometer; Finite element mesh for ABAQUS code simulations of ISO 527 standard tensile test compliance; Specimen (TR140) according to ASTM-648 for tensile testing; Tensile measurement apparatus; Specimens of Shore D hardness measures; Schematic representation of the SHORE D hardness testing device; Scanning electron microscopy was used. Design non-lethal projectile mounts with optimum physical and chemical properties; Main properties of HDPE; the MRS classification of polyethylene; common HDPE; Professional needs of the main PE80; carbon black's core characteristics; alumina core characteristics.

Statistical study: Linear regression equation for Density at 23 °C results for HDPE/CB; linear regression equation for testing MFI results for HDPE/CB mixtures; linear regression equation for testing The effects of the HDPE/CB mixture led to a lower Vicat; linear regression equation for Shore D hardness test results for HDPE/CB; linear regression equation for Izod resilience test results for HDPE/CB blends; linear regression equation for testing HDPE/CB mixtures yield strong results; linear regression equation for testing Elongation results (ε_r) in the break for HDPE/CB; linear regression equation for testing Effects of breaking strength Rr for mixtures of HDPE/CB; linear regression equation for Density at 23 °C results for HDPE/alumina mixtures is linear regression equation for MFI test results for HDPE/alumina mixtures: The linear regression equation for testing The effects of the HDPE/alumina mixture led to a lower Vicat. Linear regression equation for Shore D hardness test results for HDPE/alumina mixtures; linear regression equation for Izod resilience test results for HDPE/alumina blends; linear regression equation for testing HDPE/alumina mixtures yields strong results linear regression equation for testing elongation results (ε_r) in the break for HDPE/alumina mixtures; linear regression equation for testing Effects of breaking strength Rr for mixtures of HDPE/alumina: linear regression equation for testing The residual masses and degradation temperatures for different mixtures of HDPE: Δm (m_f–m_0) (mg), loss at the end of the process (%), residue at 500 °C (%), $T_{d\max}$ (°C), The linear regression equation for the DSC test determines the glass transition temperature and melting temperatures of our HDPE: T_g °C, T_m °C, T_C %, ΔH_f J/g, T_c °C, ΔH_c J/g, the appendix for the Linear Programming class in Carbon Black: Matrix, Matrix solution, Matrix ganging, Appendix for the Linear Programming matrix for alumina: Matrix, Matrix solution, Matrix ganging, Appendix

for the Linear Programming matrix for pure HDPE: Matrix, Matrix solution, Matrix ganging; CODE STATA.

Supplementary materials: These include a detailed work methodology flowchart, as well as supplementary tables and figures that elaborate on the material properties and experimental methods. Key tables display the physical properties of high-density polyethylene (HDPE), such as its density, crystallinity, melting temperature, and glass transition temperature, along with the MRS classification and common types of HDPE. We also provide additional information about the core characteristics of carbon black (CB) and alumina, emphasizing their impact on the mechanical and thermal properties of HDPE nanocomposites. The statistical study section presents equations and analyzes test results, looking at how different amounts of carbon black and alumina fillers affect the density, melt flow index (MFI), Vicat softening point, Shore D hardness, and Izod impact resistance of HDPE composites. These linear regressions offer clues about the relationships between filler content and the material properties of the HDPE/CB and HDPE/alumina mixtures. These supplementary materials are instrumental in supporting the research findings and providing additional clarity regarding the experimental methodology, results, and analysis.

Author contributions: Conceptualization, DRJ; methodology, DRJ; software, DRJ; formal analysis, BN; investigation, BN; resources, BN; data curation, DRJ; writing—original draft preparation, BN; writing—review and editing, BN and GJF; visualization, GJF; supervision, GJF; project administration, GJF; funding acquisition, BN. All authors have read and agreed to the published version of the manuscript.

Acknowledgments: Thank you to the IMP laboratory (Polymer Materials Engineering), UMR CNRS 5223, National Institute of Applied Sciences of Lyon (INSA Lyon). IMP Laboratories offered me an ideal working environment during these internship periods.

Conflict of interest: The authors declare no conflict of interest.

References

1. Kaplan WA. Modern Plastics Encyclopedia. Mcgraw-Hill/Modern Plastics; 1998.
2. Bielinski D, Lipinski P, Slusarski L, et al. Surface layer modification of ion bombarded HDPE. Surface Science. 2004; 564: 179–186.
3. Boumdouha N, Safidine Z, Boudiaf A, et al. Experimental study of the dynamic behavior of loaded polyurethane foam free fall investigation and evaluation of microstructure. The International Journal of Advanced Manufacturing Technology. 2022; 120: 3365–3381. doi: 10.1007/s00170-022-08963-1
4. Chen X, Xu Y, Cao X, Gubanski SM. Electrical treeing behavior at high temperature in XLPE cable insulation samples. IEEE Transactions on Dielectrics and Electrical Insulation. 2015; 22: 2841–51.
5. Boumdouha N, Courty L, Duchet-Rumeau J, Gerard JF. Quasi-Static Compression and Microstructural Characterization of Polyurethane Foams for Potential Use in Shock Absorbers. Journal of Basic & Applied Sciences. 2024; 20: 23–33.
6. Vaughan AS, Zhao Y, Barré LL, et al. On additives, morphological evolution and dielectric breakdown in low density polyethylene. European Polymer Journal. 2003; 39: 355–65.
7. Boumdouha N, Safidine Z, Boudiaf A, et al. Manufacture of polyurethane foam with a certain density. In: Proceedings of the International Conference on Recent Advances in Robotics and Automation ICRARE'18; 3–4 November 2018; Monastir, Tunisia. pp. 21–30.
8. Saci H, Bouhelal S, Bouzarafa B, et al. Reversible crosslinked low density polyethylenes: Structure and thermal properties.

Journal of Polymer Research. 2016; 23: 1–9.
9. Huang JL, Nayak PK. Strengthening alumina ceramic matrix nanocomposites using spark plasma sintering. In: Advances in Ceramic Matrix Composites. Elsevier; 2018. pp. 231–247.
10. Streller RC, Thomann R, Torno O, Mulhaupt R. Isotactic poly (propylene) nanocomposites based upon boehmite nanofillers. Macromolecular Materials and Engineering. 2008; 293: 218–227.
11. Streller RC, Thomann R, Torno O, Mulhaupt R. Morphology, crystallization behavior, and mechanical properties of isotactic poly (propylene) nanocomposites based on organophilic boehmites. Macromolecular Materials and Engineering. 2009; 294: 380–388.
12. Siengchin S, Karger-Kocsis J, Thomann R. Nanofilled and/or toughened POM composites produced by water-mediated melt compounding: Structure and mechanical properties. Express Polymer Letters. 2008; 2: 746–756.
13. Yang JL, Zhang Z, Schlarb AK, Friedrich K. On the characterization of tensile creep resistance of polyamide 66 nanocomposites. Part I. Experimental results and general discussions. Polymer. 2006; 47: 2791–801.
14. Karger-Kocsis J, Kmetty Á, Lendvai L, et al. Water-assisted production of thermoplastic nanocomposites: A review. Materials. 2015; 8: 72–95.
15. Siengchin S, Karger-Kocsis J. Mechanical and stress relaxation behavior of Santoprene® thermoplastic elastomer/boehmite alumina nanocomposites produced by water-mediated and direct melt compounding. Composites Part A: Applied Science and Manufacturing. 2010; 41: 768–773.
16. Boumdouha N, Safidine Z, Boudiaf A. Preparation of Nonlethal Projectiles by Polyurethane Foam with the Dynamic and Microscopic Characterization for Risk Assessment and Management. ACS Omega. 2022; 7: 16211–16221.
17. Noureddine B, Achraf B, Zitouni S. Mechanical and chemical characterizations of filled polyurethane foams used for non-lethal projectiles. In: Proceedings of the 10-th European Symposium on Non-Lethal Weapons EWG-NLW; 20–23 May 2019; Brussels, Belgium. p. 68.
18. Boumdouha N, Duchet-Rumeau J, Gerard JF et al. Research on the Dynamic Response Properties of Nonlethal Projectiles for Injury Risk Assessment. ACS Omega. 2022; 7: 47129–47147.
19. Boumdouha N, Duchet-Rumeau J, Gerard JF. Enhancement of Mechanical Properties in Non-Lethal Projectile Holders through High-Density Polyethylene and Alumina Nanocomposites. Journal of Basic & Applied Sciences. 2024; 20: 34–47.
20. Boumdouha N, Safidine Z, Boudiaf A. Experimental Study of Loaded Foams During Free Fall Investigation and Evaluation of Microstructure. The International Journal of Advanced Manufacturing Technology. 2021.
21. Boumdouha N, Duchet-Rumeau J, Gerard JF. Structure Property and Performance of Polymeric Foams: A Review. Journal of Basic & Applied Sciences. 2024; 20: 1–22.
22. Trotignon JP, Piperaud M, Verdu J, Dobraczynski A. Summary of plastic materials, Structure–Properties, Implementation and Standardization (French). Afnor; 1992.
23. Chaudhuri I, Ngiewih Y, McCunney RJ, Levy L. Carbon black is not black carbon. Toxicological & Environmental Chemistry. 2021; 103: 236–237.
24. Namdari M, Lee CS, Haghighat F. A systematic comparative study of granular activated carbons and catalysts for ozone removal. Building and Environment. 2022; 224: 109510.
25. Jebur SK. Carbon black production, analyzing and characterization [Master's thesis]. Missouri University of Science and Technology; 2018.
26. Yuan Q, Jiang W, An L, et al. Mechanical and thermal properties of high-density polyethylene toughened with glass beads. Journal of Applied Polymer Science. 2003; 89: 2102–2107.
27. Zhang S, Cao XY, Ma YM, et al. The effects of particle size and content on the thermal conductivity and mechanical properties of Al_2O_3/high density polyethylene (HDPE) composites. Express Polymer Letters. 2011; 5: 581–590.
28. Saxena PK, Raut KG, Srinivasan SR, et al. Polyurethane waterproofing coating for building applications. Construction and Building Materials. 1991; 5: 208–210.
29. ASTM D. 1505-03—Standard Test Method for Density of Plastics by the Density-Gradient Technique. American Society for Testing and Materials; 2003. pp. 1–7.
30. Alimi L, Ghabeche W, Chaoui W, Chaoui K. Study of the mechanical properties through the wall of an extruded HDPE-80 tube intended for the distribution of natural gas (French). Matériaux & Techniques. 2012; 100: 79–86.
31. Shirsath NB, Gupta GR, Gite VV, Meshram JS. Studies of thermally assisted interactions of polysulphide polymer with ionic liquids. Bulletin of Materials Science. 2018; 41: 1–8.

32. Hemminger W. Thermal Analysis: Fundamentals and Applications to Polymer Science. Thermochimica Acta; 1995.
33. Lewitus D, McCarthy S, Ophir A, Kenig S. The effect of nanoclays on the properties of PLLA-modified polymers Part 1: Mechanical and thermal properties. Journal of Polymers and the Environment. 2006; 14: 171–177.
34. Dali-Youcef Z, Bouabdasselem H, Bettahar N. Removal of Organic Compounds by Local Clays (French). Comptes Rendus Chimie. 2006; 9: 1295–1300.
35. Gaboune A. Use of polymerization compounding technique for the preparation of polyethylene/montmorillonite nanocomposite (French) [Master's thesis]. Université Laval; 2006: 37.
36. Peterlin A. Mechanical properties of fibrous structure. extrait de «Ultra-Hight modulus polymers». Gifferi A, Ward IM. London: Appl. Sic. Pub. Ltd. 1979; 279–320.
37. Ward IM. The yield behavior of polymers. Journal of materials Science. 1971; 6: 1397–417.
38. Faerber J. Scanning electron microscopy X-ray microanalysis by electron probe (French). Institut de Physique et Chimie de Matériaux de Strasbourg (IPCMS); 2004. pp. 1–53.
39. Hassan EAM, Elarabi SE, Wei Y, Yu M. Biodegradable poly (lactic acid)/poly (butylene succinate) fibers with high elongation for health care products. Textile Research Journal. 2018; 88: 1735–1744.
40. Ling GH, Shaw MT. Crystalline crosslinked microparticles from immiscible blends of polyethylene and polystyrene. Polymer. 2009; 50: 4917–4925.
41. Bocchini S, Morlat-Thérias S, Gardette JL, Camino G. Influence of nanodispersed boehmite on polypropylene photooxidation. Polymer Degradation and Stability. 2007; 92: 1847–1856.
42. Fu T. PP/clay nanocomposites: compounding and thin-wall injection moulding [Doctoral dissertation]. Loughborough University; 2017.
43. Choi WJ, Kim SH, Jin Kim Y, Kim SC. Synthesis of chain-extended organifier and properties of polyurethane/clay nanocomposites. Polymer. 2004; 45: 6045–6057.
44. Lai SM, Chen WC, Zhu XS. Melt mixed compatibilized polypropylene/clay nanocomposites: Part 1—the effect of compatibilizers on optical transmittance and mechanical properties. Composites Part A: Applied Science and Manufacturing. 2009; 40: 754–765.
45. Ashby MF, Jones DRH. Materials. Volume 2, Microstructure and Implementation (French). Dunod; 1997.
46. Osswald TA. Mechanical Behavior of Polymers. Understanding Polymer Processing. 2017: 29–59.
47. Leszczyńska A, Njuguna J, Pielichowski K, Banerjee JR. Polymer/montmorillonite nanocomposites with improved thermal properties. Part I. Factors influencing thermal stability and mechanisms of thermal stability improvement. Thermochimica Acta. 2007; 453: 75–96.
48. Guermazi N, Elleuch K, Ayedi HF, Kapsa P. Aging effect on thermal, mechanical and tribological behavior of polymeric coatings used for pipeline application. Journal of Materials Processing Technology. 2008; 203: 404–410.
49. Liang G, Xu J, Bao S, Xu W. Polyethylene/Maleic anhydride grafted polyethylene/organic-montmorillonite nanocomposites. I. Preparation, microstructure, and mechanical properties. Journal of Applied Polymer Science. 2004; 91: 3974–3980.
50. Dabees S, Tirth V, Kamel BM. Synthesis and characterization studies of high-density polyethylene-based nanocomposites with enhanced surface energy, tribological, and electrical properties. Polymer Testing. 2021; 98: 107193.
51. Usuki A. Nylon 6-clay Hybrid: From Invention to Practical Use. R&D Review of Toyata CRDL. 2016; 47(1): 45–55.
52. Noureddine B, Zitouni S, Achraf B, et al. Development and Characterization of Tailored Polyurethane Foams for Shock Absorption. Applied Sciences. 2022; 12: 2206.
53. Boumdouha N, Safidine Z, Boudiaf A, et al. Mechanical and microstructural characterization of polyurethane foams. In: Proceedings of the 8th Chemistry Days JCh8–EMP; 26–27 March 2019; Algiers, Algeria. p. 169.
54. Boumdouha N, Safidine Z, Boudiaf A. A new study of dynamic mechanical analysis and the microstructure of polyurethane foams filled. Turkish Journal of Chemistry. 2022; 46: 814–834.
55. Boumdouha N, Louar MA. Influence of Microstructure on the Dynamic Behavior of Polyurethane Foam with Various Densities. Journal of Basic & Applied Sciences. 2023; 19: 131–150.